Molecular-dynamics simulation of lattice thermal conductivity in $Pb_{1-x}Sn_xTe$ and $Pb_{1-x}Ge_xTe$ at high temperature

T. Chonan and S. Katayama*

School of Materials Science, Japan Advanced Institute of Science and Technology,

1-1 Asahidai, Nomi, ishikawa 923-1292, Japan

*e-mail address: s-kata@jaist.ac.jp

Abstract

The molecular-dynamics studies on lattice thermal conductivity (κ_L) of $Pb_{1-x}Sn_xTe$ and $Pb_{1-x}Ge_xTe$ are carried out by employing ion model potential for mutual ion-ion interactions at the average temperatures 300 and 500 K under non-equilibrium condition. Special emphasis of investigation is on the alloying effects on κ_L by changing the alloying content x of Sn and Ge in PbTe. It has been shown that a remarkable reduction of κ_L at finite x is demonstrated in $Pb_{1-x}Sn_xTe$ and $Pb_{1-x}Ge_xTe$ without a relying on a phonon scattering description. We have compared our results with ones evaluated by the Abeles' formula of lattice thermal conductivity due to phonon scattering from alloy fluctuations.

KEYWORDS: lattice thermal conductivity, molecular-dynamics simulation, PbTe alloys

I. Introduction

Recently, there has been a great deal of interest to find high-efficiency thermoelectric materials with a large thermoelectric figure of merit $Z = \sigma S^2 / \kappa$ where σ is the electric conductivity, S the Seebeck coefficient, and $\kappa (= \kappa_e + \kappa_L)$ the thermal conductivity consisting of electronic (κ_e) and lattice part (κ_L). Since the suggestion by Ioffe *et al.*[1] a reduction of κ_L is one of the possible ways to attain high Z because of the limited value of κ_e due to its constant ratio to σ. Thus low κ_L as well as high S and σ were important ingredients to find and synthesize new thermoelectric materials such as skutterudites and clathrates so far.[2] PbTe-based alloys have been studied widely as the thermoelectric materials in the medium temperature range (300-900 K). The alloying of PbTe with SnTe and GeTe containing various defects has been exploited to control the number of carriers, the type of carrier conduction from n-type to p-type or vice versa, in addition to produce the change of carrier mobility as well as to reduce κ_L. Even for these established thermoelectric materials, new theoretical approach, i.e. carrier pocket engineering[3] to lead an optimum value of ZT has been introduced related to the design of artificial superlattices (SLs) fabricated by the molecular beam epitaxy (MBE) method. The theory has been tested by a measurement of power factor σS^2 in many semiconductors SLs such as PbTe/PbEuTe[4], Si/Ge[5], and GaAs/AlAs.[5] Further data of PbSeTe/PbTe quantum dot superlattice structures exhibit ZT~1.6 at 300 K, and suggest the importance of much lower κ_L.[6] So it is required to clarify the role of the phonon scattering from

alloy fluctuations as well as phonon – interface scattering in the artificial nano-systems to design more efficient structures. The theoretical treatment of bulk lattice thermal conductivity at entire temperatures has been developed for a long time by taking into account the phonon-phonon, phonon-point defect, and phonon-boundary scatterings.[7] However, these theories contain many unknown physical quantities such as the anharmonic potentials and coupling strength between phonon and point-defect. Also note that new materials with low κ_L such as clathrates show up for which phonon picture is not applicable because of highly relaxed systems due to the existence of rattlers.[8] New concept of "phonon glass and electron crystal"[9] has been proposed. Thus these situations have required a different new approach to evaluate κ_L without relying on the phonon scattering description.

In this paper we present a classical non- equilibrium molecular-dynamics (NEMD) study of lattice thermal conductivity at high temperature with use of an ideal insulating ionic model for $Pb_{1-x}Sn_xTe$ and $Pb_{1-x}Ge_xTe$. To determine the model potential and structure parameters in the present NEMD simulation, the equilibrium molecular dynamics (EMD) method has been adopted first which was developed to explore the local structure o $Pb_{1-x}Ge_xTe$ and $Pb_{1-x}Sn_xTe$ by one of the present authors and his collaborators. [10]

In § 2, we examine the local structure of PbSnTe and PbGeTe alloy by calculating the pair correlation function using the EMD method. The main contribution of this paper is embedded in

§ 3. In § 3-1, we first study the temperature and system size dependence of κ_L in PbTe by assuming a simple model for κ_L which contains the effective phonon mean free path. We find the significant limitation of mean free path due to the phonon scattering from the heating and cooling layers, when mean free path due to phonon-phonon scattering becomes comparable order with system size. In § 3-2(a), we present the NEMD results concerning to alloy effects on κ_L of $Pb_{1-x}Sn_xTe$ and $Pb_{1-x}Ge_xTe$ at temperatures 300 and 500 K . We find strong reduction of κ_L as increasing the content of Sn and Ge in PbTe. We mention the difference of κ_L between PbSnTe and PbGeTe due to the difference of local lattice relaxation related to the difference of ion size among Pb^{2+}, Ge^{2+}, and Sn^{2+}. The § 3-2(b) will be devoted to the detailed discussion of alloying effects on κ_L in comparison with the phonon scattering from alloy fluctuations estimated by using Abeles' formula.[11] In final section 4, the summary and concluding remarks is given by considering future probable application of classical NEMD calculation for κ_L.

2. MD simulation of local structure in PbSnT and PbGeTe alloys

The narrow-gap semiconductor alloys PbSnTe and PbGeTe have been widely studied as materials for both infrared photo-detector devices and infrared semiconductor lasers, in addition to the thermoelectric materials. They have also attracted our attentions due to the ferroelectric phase transition from cubic NaCl to rhombohedral structures at critical temperature T_c. Therefore, this

incipient ferroelectric property plays an important role to provide high carrier mobility even in the high alloy contents because the high lattice dielectric constant screens strongly the ionized defect potentials for carriers. This might be one of the reasons that PbTe alloys are good thermoelectric materials. A sequence of experimental studies of alloy effects on the structural change has elucidated that PbSnTe behaves like a simple alloy, while PbGeTe exhibits anomalous change of T_c as a function of Ge^{2+} content deviating from the ideal alloys.[12] It was shown that such characteristics of phase change in PbGeTe are attributed to the off-center instability of Ge^{2+} substituted in Pb sites.[13] So it is expected that the difference of ion sizes among Pb^{2+}, Sn^{2+} and Ge^{2+} influences much κ_L. Here, we determine first some parameters of pair potential needed for NEMD of thermal conductivity by calculating pair correlation function of alloys using EMD.[10]

The molecular dynamics simulation is performed using MXDORTO[14] by modifying the program in which the disorder substitution of Ge^{2+} and Sn^{2+} for Pb^{2+} ions is produced by application of random numbers. In MD calculation, we suppose that all pseudobinary systems have cubic rocksalt structure, space group Fm3m, because rhombohedral PbGeTe (T_c = 650 K) distorts slightly from cubic NaCl structures above 300 K. We have adopted the effective Coulomb ionic potential function between ions, i and j as

$$u_{ij}(r) = \frac{Z_i Z_j}{r} + f_0(b_i + b_j)\exp[\frac{a_i + a_j - r}{b_i + b_j}], \qquad (1)$$

where r is the distance between ions, Z_i is the ionic charge, and a and b are the effective radius and softness parameter of the i-th ions with the standard force f_0, respectively. We assume that $Z_{Pb,Sn,Ge} = +2$, Z_{Te} = -2 and $f_0 = 1$ kcal mol^{-1}Å^{-1}. The basic MD cell was rectangular box with $\ell \times m \times n$ as shown in Fig. 1 where the half of the cubic lattice constant (d= cubic lattice constant /2) of NaCl structure is chosen as the length unit. So the length of MD cell along x-, y- and z-axis are $L_x = \ell d$, $L_y = md$, and $L_z = nd$. Thus a single layer in the zx plane assigned by m contains 32 cations and 32 anions so that this layer involves 64 ions. In Fig. 1, we draw also the heating slab (source) and the cooling thin slab (sink) schematically which are set at $L_y / 4$ and $3L_y / 4$. We carry out first the EMD by using $\ell = 4, m = 64$ and $n = 4$ in zero heating and cooling, so that total number of atoms is 4096. The long-range Coulomb portion of potential is calculated using the Ewald summation technique. The total MD step is assumed to be 20000 with unit time step Δt = 0.8 fs for attaining the equilibrium state. We calculate the pair correlation function from location of each atom which is obtained by averaging data taken from the final 2000 steps. The parameters in potential are estimated by fitting the lattice parameters with the observed one at 300 K and 0.0001 GPa for PbTe, SnTe and GeTe. The values of a_i are $a_{Pb} = 1.450$ Å, $a_{Ge} = 0.966$ Å, $a_{Sn} = 1.300$ Å and $a_{Te} = 2.352$ Å. The parameter b is assumed to be 0.08 Å for all species of ions.

In Fig. 2(a) and (b), we plotted pair correlation functions $g_{i-j}(r)$ for (i-j) pair of atoms. In Fig. 2(a) we show $g_{i-j}(r)$ of $Pb_{1-x}Sn_xTe$ with x =0, 0.3, 0.6 and 1.0 at 300 K whereas the pair correlation

functions of $Pb_{1-x}Ge_xTe$ at 300 K are depicted in Fig. 2(b). The local relaxed structure associated with each ion is monitored by these functions. It is evident that the location of the first peak in $g_{Pb-Te}(r)$, $g_{Sn-Te}(r)$ and $g_{Ge-Te}(r)$ agrees with the distance from the first-neighbor Te distance in cubic structures within 0.02 Å so that the present MD technique reproduces well cubic PbTe and SnTe, and pseudocubic GeTe at 300 K. In comparison between those of Fig. 2(a) and (b), we can see that g_{Ge-Te} and g_{Te-Te} in PbGeTe distributes widely while g_{Te-Sn} is quite sharp. The peak of g_{Te-Pb} in both alloys exhibits a small shift corresponding to the averaged change of lattice constant as x increases. These features are consistent with the EXAFS results of $Pb_{1-x}Ge_xTe$ (x~0.3) by Ravel et al.[15] They have pointed out that the structure disorder of PbGeTe is accommodated only by the local distortion of Ge^{2+} and Te^{2+} sublattices, while Pb^{2+} sublattice distortion is not efficient. In the consequence by this calculation, we find that PbGeTe has more relaxed local structure than PbSnTe. By this MD method, the binding energies of PbTe, SnTe and GeTe are estimated to be -29.4, -30.7 and -32.4 eV/molecule, respectively. The experimental values of these compounds are -31.4, -31.89 and -34.2 eV/molecule, respectively.[16] The agreement is fairly good even in the present simple ionic model.

3. NEMD simulation of lattice thermal conductivity of PbSnTe and PbGeTe

The lattice thermal conductivity is evaluated by means of the NEMD method with use of the Fourier's law as

$$J_y = -\kappa_L \frac{dT}{dy}, \qquad (2)$$

by assuming a heat flow along the [010] cubic crystal axis. In the present analysis we consider the source and sink consisting of the two-layers. By rescaling velocities of particles in the source and sink region at each MD step Δt, heat $\Delta\varepsilon$ is added in heat source, and is removed from heat sink, respectively. This means that each particle velocity in these regions is scaled by the same factor so that the resulting net kinetic energy is increased (decreased) by amount $\Delta\varepsilon$ in source (sink). The equilibration between kinetic and potential energy takes place within a typical vibrational period (<1ps), so the system achieves steady state and the local temperature is defined. Thus the heat current is given by $J_y = \Delta\varepsilon / 2A\Delta t$, and κ_L is estimated by the Fourier's law with the temperature gradient. We follow the NEMD recipe to calculate κ_L which have been developed in various works.[17-19)]

(1) In order to arrange coordinate and velocity of each particle in equilibrium state, the EMD calculation has been carried out by the Nose's method in the first 2000 steps with Δt =0. 8 fs.

(2) After the above EMD, the NEMD is started by adding and subtracting $\Delta\varepsilon$ per unit MD step due to the velocity modification of particles in the source and sink.

(3) When the instantaneous temperature $T_{N-j}(md)$ at y=md for the N-j time step is given by

$$3k_B T_{N-j}(md) = \frac{1}{N_m}\sum_i m_i v_i^2 (N-j), \qquad (3)$$

an average of T_{N-j} over the final M time steps is written as

$$T(md) = \frac{1}{M}\sum_{j=0}^{M-1} T_{N-j}(md). \qquad (4)$$

In eq.(3), $v_i(N-j)$ is the magnitude of velocity of the i-th particle in the m-th layer with mass m_i at the N-j time step, N is the total number of steps in the simulation, and N_m is the number of ions in m-th layer. As long as M is small compared with N, the average of $T_{N-j}(md)$ could not take into account the transient effects related to the heat source. By the above procedure, we find the local temperature at each layer in the simulation cell. So we could estimate the temperature gradient from the temperature profile.

(4) To confirm the achievement of the steady state, we check the dependence of κ_L on N. If κ_L approached one independent of N almost, we may regard it as the stationary value of κ_L.

By this way, we explore the stationary value of κ_L for L_y = 208 Å at 300 and 500 K assuming $\Delta\varepsilon / k_B = 0.1$ K and M= 2000 by changing N from 22000 to 62000. In Fig. 3, we plot our results (solid circles at 300 K and solid squares at 500 K). From this result, we choose N= 42000 from both the reasonable results and reduction of computing time. In Fig. 4(a) and (b), we plot the temperature profile as a function of layer number m along the y-axis at T= 500 K for length 208 Å

and 416 Å of PbTe by using N= 42000. Insets show the least square linear fit to the data for appropriate length along y-axis.

3-1 Temperature and system size dependence of κ_L of PbTe

In the phonon description of insulating crystals, it is well known that the temperature dependence of κ_L at $T > \theta_D$ is attributed to the third order Umklapp phonon-phonon scattering processes. On the other hand, the boundary scattering becomes important for κ_L at low temperatures. However, it has been recognized that the boundary scattering contributes κ_L within a finite size material even in high temperatures when the bulk phonon mean free path becomes a comparable order to the system size in nanostructured materials such as thin-films and multi-layered system. From the view of NEMD calculation, the system size is also a key ingredient to determine the computing time and to produce the scattering from source and sink. Thus the simulation cell size is determined by the competition between the complexity due to scattering from source and sink and a reduction of computing time.

In the present work, we employ the simple kinetic theory of thermal conductivity in order to analyze our computed results. Thermal conductivity due to the kinetics of phonon carriers is expressed in general by $\kappa_L = c_v v_s \ell_{eff} / 3$ with specific heat c_V and average sound velocity v_s as well as effective mean free path ℓ_{eff}. So the temperature and system size dependent of thermal conductivity at high temperature is attributed to ℓ_{eff}. The inverse of it consists of two portions as

$$\frac{1}{\ell_{eff}} = \frac{1}{\ell_{\infty}} + \frac{4}{L_y}. \qquad (5)$$

This form was discussed carefully by Schelling et al.[19] In their discussion, the mean free path related to the scattering from the source and sink is considered to be $L_y / 4$.

(a) Temperature dependence of κ_L

Figure 5 shows κ_L versus $1/T$. The solid circles and solid squares give the MD results for $L_y = 208$ and 416 Å at 300 and 500 K. To analyze the above data, we rewrite the previous kinetic formula of κ_L as

$$\kappa_L(T) = \frac{\kappa_{bL}(T)}{1 + \frac{4}{L_y}\ell_b(T)}, \qquad (6)$$

with $\kappa_{bL} = c_v v_s \ell_b(T)/3$. The denominator expresses a correction due to the scattering from heating and cooling layers. Since κ_{bL} = D/T, $D = 3.5(k_B/h)^3 M V^{1/3} \theta_D{}^3 / \gamma^2$ [20] in high temperature range, D is estimated to be D= 2986 (W/m) using θ_D =130K and γ = 1.45 for PbTe. The calculated results of eq.(6) are depicted by dashed and dash-dotted line for $L_y = 208$ Å and 416 Å so as to fit the data of $L_y = 208$ Å at 500 K. It is demonstrated that the phonon scattering from the source and sink reduces much κ_L from the κ_{bL} line. The estimated bulk mean free path is $\ell_b(T = 500K) = 53$ Å. Using this value, we also find $\ell_b(T = 300K) = 88$ Å.

(b) System size dependence of κ_L

In Figs. 6(a) and (b), we plot $1/\kappa_L$ (solid circles and solid squares) versus $1/L_y$ at 300 and 500 K in twelve samples with different system size from 168 to 416 Å. The solid lines denote the least

square linear fit for the data at 300 and 500 K, respectively. From eq.(1) and eq.(4), we can find ℓ_b in the limit of $1/L_y \to 0$. The values of ℓ_b are estimated to be 187.5 and 71.5 Å at 300 and 500 K, respectively. Although we obtain a little different value of ℓ_b compared with ones from the temperature dependence, this may attributed to the scattered data in $1/\kappa_L$ for $1/L_y > 0.0058$ because of the possibility of occurrence of ballistic conduction in such small size system.

3-2. Alloy effects on lattice thermal conductivity of $Pb_{1-x}Sn_xTe$ and $Pb_{1-x}Ge_xTe$

(a) NEMD results

We present the alloy effects on κ_L of $Pb_{1-x}Sn_xTe$ and $Pb_{1-x}Ge_xTe$ based on the NEMD method using the same potential parameters with EMD in §2, $\Delta\varepsilon/k_B$ = 0.1K, L_y = 208Å, N=42000, and M= 2000. In Fig. 7 (a) and (b), our calculated temperature profile is shown for $Pb_{1-x}Sn_xTe$ and $Pb_{1-x}Ge_xTe$ as a function of layer number m at 300 K for x=0, 0.3, 0.6 and 1.0. The temperature feature is relatively smooth, except for some change of local temperatures at several points. The difference $\Delta T=(T_h-T_L)$ between the highest temperature (T_h) in source and the lowest one (T_L) in sink in Fig. 7(a) changes from 160.2, 322.0, 219.0 and 109.3 corresponding to x=0.0, 0.3, 0.6 and1.0 in $Pb_{1-x}Sn_xTe$, while ΔT varies160.2, 326.9, 349.5, and 133.7 corresponding to x=0.0, 0.3, 0.6 and 1.0 in $Pb_{1-x}Ge_xTe$. These differences illustrate the characteristics of heat conduction in compounds and alloys. The insets show the least square linear fit to data which are taken between

m=25 and 39 including the center point of the system. From this fit, we estimate the temperature gradient of alloys. In Fig. 8(a) and (b), we plot the calculated κ_L by solid circles as a function of alloy content x. We can see that κ_L in alloys is reduced much to one-third values in compound. It is also evident that κ_L of $Pb_{1-x}Ge_xTe$ is steeply reduced as Ge content x increases, while κ_L of $Pb_{1-x}Sn_xTe$ is gradually decreased. We can see that the reduced κ_L in alloys at 300 and 500 K exhibits almost the same value in alloys, in spite of the clear difference of κ_L in PbTe, SnTe and GeTe at 300 and 500 K. This means that lattice thermal conductivity in $Pb_{1-x}Sn_xTe$ and $Pb_{1-x}Ge_xTe$ is very much dominated by the scattering from alloy fluctuations.

(b) Comparison of MD results with κ_L from phonon picture

The alloying effects on lattice thermal conductivity of a disordered semiconductor have been studied at first by Abeles. [11] He developed a theory of phonon-point defect scattering by Klemens[21] and Callaway'theoy[22] which focused the normal phonon-phonon scattering in order to produce an increase of phonon population at high energy. Since the high energy phonon is scattered by point defect and strain more efficiently efficiently, the thermal resistivity is increased. Abeles has applied his theory the thermal resistivity calculation in Si-Ge and In(Ga)As and Ga(In)P. Here we compare our results with the one evaluated by Abeles's formula eq.(22) in his paper. We first transform from his thermal resistance formula to $\kappa_L(x)$ for $A_{1-x}B_x$ alloys as

$$\kappa_L(x) = \frac{\kappa_L^{av}}{(1+(5\alpha/9)}[\frac{\tan^{-1}U}{U} + \frac{(1-(\tan^{-1}U/U))^2}{[(1+\alpha)/5\alpha]U^4 - U^2/3 + 1 - (\tan^{-1}U/U)}], \quad (7)$$

where α is the ratio between relaxation rates of the Normal and Umklapp processes, and

$$U^2(1+(5/9)\alpha = (9\pi/2)^{1/2}\pi^2\delta^{av}\Gamma\kappa_L^{av}/\theta_D^{av}. \qquad (8)$$

The important factor Γ is related to the disorder scattering from mass defect and lattice strains as

$$\Gamma = x(1-x)[(\Delta M/M^{av})^2 + \varepsilon(\Delta\delta/\delta^{av})^2], \qquad (9)$$

with $\Delta M = M_A - M_B, \Delta\delta = \delta_A - \delta_B$. The average quantities denoted by Q^{av} in eqs.(8) and (9) is given by

$$Q^{av} = (1-x)Q_A + xQ_B. \qquad (10)$$

In the use of Abeles' formula, we assume κ_L (x=0) in PbTe, κ_L (x=1) of SnTe and GeTe estimated by the present NEMD and $\alpha = 2.5$, $\varepsilon = 39$ and $\theta_D = 130$, 152 and 168 K for PbTe, SnTe and GeTe. In Figs. 8(a) and (b), the dashed lines correspond to the Abeles' results. We plot also κ_L for $\varepsilon = 0$ by dash-dotted lines. It is quite interesting that the magnitude of reduction is almost same to ones of MD calculation, even though the parameters for III-V compound alloys are used. From the comparison between dashed and dashed-dotted line, it is seen that the scattering from mass defects dominates the alloy scattering. We can see the significant asymmetric variation in the NEMD result κ_L as a function of x. This variation is opposite to the Abeles' one that comes from the differences of κ_L among PbTe, SnTe and GeTe. The fundamental variation of Abeles' one comes from the x(1-x) dependece in Γ. That is, the scattering from lattice strain as well as of mass difference is taken into account in the averaged fashion (i.e. virtual crystal). This suggests us that

the large difference in x-variation of κ_L between NEMD results and Abeles' one is ascribed to the local lattice distortion depending on the alloy contents. This local distortion deviating from the average change may be produce by the large difference of ion sizes among Ge^{2+}, Sn^{2+} and Pb^{2+} ions.

4. Concluding Remarks

We have developed a classical non-equilibrium molecular dynamics (NEMD) simulation of lattice thermal conductivity in $Pb_{1-x}Sn_xTe$ and $Pb_{1-x}Ge_xTe$ alloys. To determine the potential parameters needed in the NEMD calculation, we explore the pair correlation functions in $Pb_{1-x}Sn_xTe$ and $Pb_{1-x}Ge_xTe$ so as to reproduce the cubic lattice constant in PbTe, SnTe and GeTe at 300 K. Our simulated pair correlation functions correspond well to the observed EXAFS data of $Pb_{1-x}Ge_xTe$ (x~ 0.3). We have analyzed the temperature and system size dependence of κ_L in PbTe by using a simple model with the inverse of effective mean free path consisting of bulk phonon scattering and scattering from the source and sink. As a consequence of the analysis, we have pointed out the existence of remarkable scattering from heat source and sink in our model system. The estimated bulk mean free path is about 50 ~ 100 Å which are comparable to the system size adopted in the present NEMD. Further, we have examined the alloying effects on κ_L in $Pb_{1-x}Sn_xTe$ and $Pb_{1-x}Ge_xTe$, and have revealed remarkable reduction of κ_L. In comparison of Abeles' theory by phonon picture with the NEMD results, we find a significant difference between them in both Pb_{1-}

$_{x}Sn_{x}Te$ and $Pb_{1-x}Ge_{x}Te$. These differences come from the local alloy fluctuation deviated from average behavior of alloys (virtual crystal) which has a x(1-x) dependence on alloy content. In the next step, we will develop the thermal conductivity theory by taking into account the pair correlations explicitly to compare the NEMD calculation. Although we could not compare explicitly our NEMD results with experiments of κ_L because of absence of relevant data in PbSnTe and PbGeTe, however, our obtained values of κ_L are quite close to the magnitude of κ_L reported in PbTe and PbSeTe,[9] and the strong reduction of κ_L due to alloyings has been observed in recent articles of PbTe-based alloys and superlattices.[23] Finally, it should be emphasized again that the present NEMD method is superior technique to evaluate κ_L in highly relaxed ionic crystals such as PbTe-based alloys.

References

[1] A.F. Ioffe, S.V. Airepetyants, A.V. Ioffe, N.V. Kolomoets, and L.S.Stil'bans, Dokl. Akad. Nauk. SSSR 106 (1956) 981.

[2] See the review article by G.S. Nolas, J. Yang, H.J. Goldsmid, in a book "Thermal Conductivity Theory, Properties, and Applications", edited. by T.M. Tritt (Kluwer Academic/Plenum Publishers, New York, Boston, Dordrecht, London, Moscow, 2004) pp. 124.

[3] See the review article M.S. Dresselhaus, Y.M. Lin, D. Dresselhasu, X. Sun, S.B. Cronin, T. Koga, J.Y. Ying, Proc. Int. Conf. on Theremoelectrics, (l999) page 92, and reference therein.

[4] L.D.Hicks, T.C. Harma, X. Sun, and M.S. Dreesselhaus, Phys.Rev. B53 (l996) R10493.

[5] T. Koga, S.B. Cronin, M.S. Dresselhaus, Mat.Res.Soc. Symp. 626(2000) Z4.3.1.

[6] T.C. Harman, P.J. Taylor, M.P. Walsh, B.E. LaForge, Science, 297 (2002) 2229.

[7] See the article by J. Yang, in Ref. [2].

[8] G.S.Nolas, T.J.R. Weakley, J.L. Cohen, and R. Sharma, Phys. Rev. B61 (2000) 3845.

[9] See the review by G. A. Slack, CRC Handbook of THERMOELEVTRICS edited by D.M. Rowe (CRC Press, Boca Raton London, New York,Washington,D.C.,l995) pp.407.

[10] S. Maruyama, S. Katayama, T. Tagawa, M. Iida, Proc. 10th Int. Conf. on Narrow gap Semicond. and Related Small Energy Phenomena, Physics, Applications, (IAPA-CS2, 2001) pp.58.

[11] B. Abeles, Phys. Rev. 131 (1963) 1906.

[12] S. Takaoka and K. Murase, Phys.Rev. B20 (l979) 2823.

[13] S. Katayama and K. Murase, Solid State Commun.36(l980) 707.

[14] K. Kawamura: Molecular Dynamics Simulation edited by F. Yonezawa (Springer-Verlag, Berlin l992) pp.88.

[15] B. Ravel, E. Cockayne, M. Newville, K.M. Rabe, Phys. Rev. B60 (l999) 14632.

[16] N.Kh Abrikosov, V.F. Bankina, L.V. Poretskaya, L.E. Shelmova and E.V.Skudnova, II-VI, IV-VI, V-VI Compounds (Plenum Press l969).

[17] C. Oligschleger and J.C. Schon, Phys. Rev. B59 (l999) 4125.

[18] P.Jund and R.Jullien, Phys. Rev. B59 (l999) 13707.

[19] P.K. Schelling, S. R. Phillpot, and P. Kebinski, Phys. Rev. B65 (2002) 024306.

[20] G.Leibfried and E. Schlomann, Nachr. Akd. Wiss. Gottingen, K1.2 Math.-Physik. 2, 71 (l954).

[21] P. G. Klemens, Proc. Phys. Soc. (London) A68 (l955) 1113.

[22] J. Callaway, Phys. Rev. 113 (l959) 1046.

[23] H.Beyer, J. Nurnus, H. Bottner, A. Lambrecht, E. Wagner, and G. Bauer, Physica E, 13 (2002) 965.

Figure Captions

Fig. 1. Schematic view of simulation cell: ℓ, m, n denote the number of unit cells along the x, y, and z axis.

Fig. 2. Pair correlation function $g_{i-j}(r)$ as a function of distance between ions, i and j . (a) $Pb_{1-x}Sn_xTe$, (b) $Pb_{1-x}Ge_xTe$ for x= 0, 0.3, 0.6, 1.0.

Fig. 3. The dependence of κ_L on the total number of MD steps N at 300 and 500 K for L_y = 208 Å.

Fig. 4. Calculated temperature profile of PbTe with system size m= 128 (416 Å) and m= 64 (208 Å) at average temperature 500 K.

Fig. 5. κ_L versus 1/T with 208 and 416 Å. The solid circles and solid squares sre the NEMD results at 300 and 500 K in PbTe. Dashed line and dash-dotted line denote the calculations using model calculation by fitting the point at 500 K for 208 Å.

Fig. 6. $1/\kappa_L$ versus 1/Ly at 300 and 500 K in twelve different PbTe with L_y from 168 to 416 Å.

Fig. 7. Temperature profile of (a) $Pb_{1-x}Sn_xTe$, (b) $Pb_{1-x}Ge_xTe$ for x= 0, 0.3, 0.6 and 1.0 at 300 K.

Fig. 8. Alloy effects on Thermal conductivity (a) $Pb_{1-x}Sn_xTe$, (b) $Pb_{1-x}Ge_xTe$. The solid circles denote the results of NEMD. The dashed line and dash-dotted line denote the calculated results by using the Abeles's formula in the presence and absence of strain scattering.

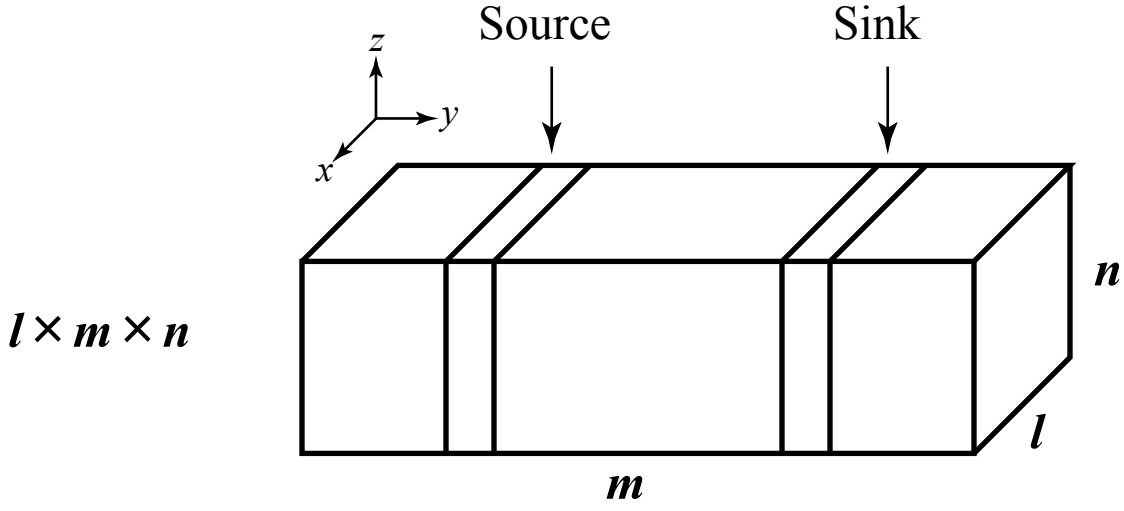

Fig.1 T. Chonan and S. Katayama

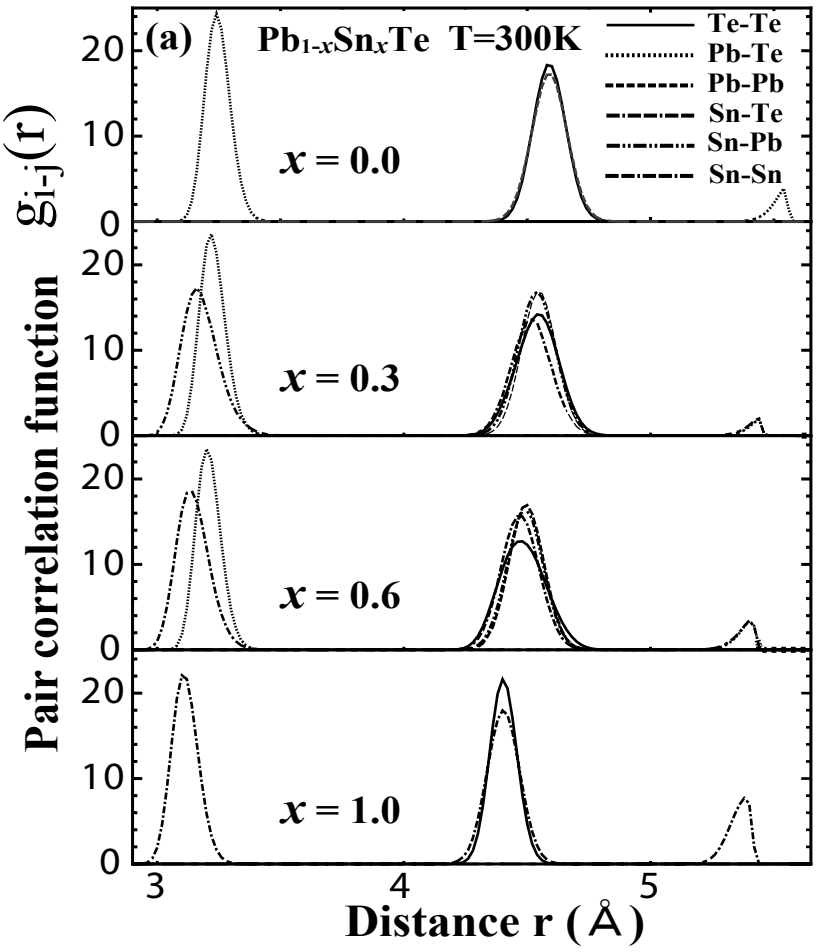

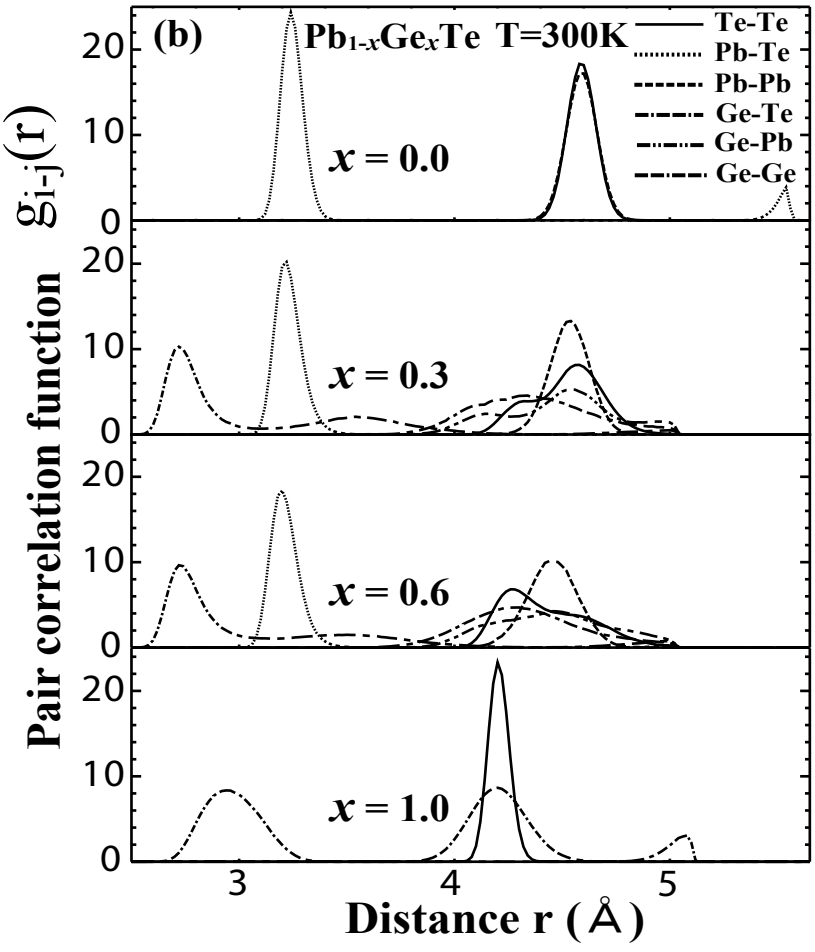

Fig.2 T. Chonan and S. Katayama

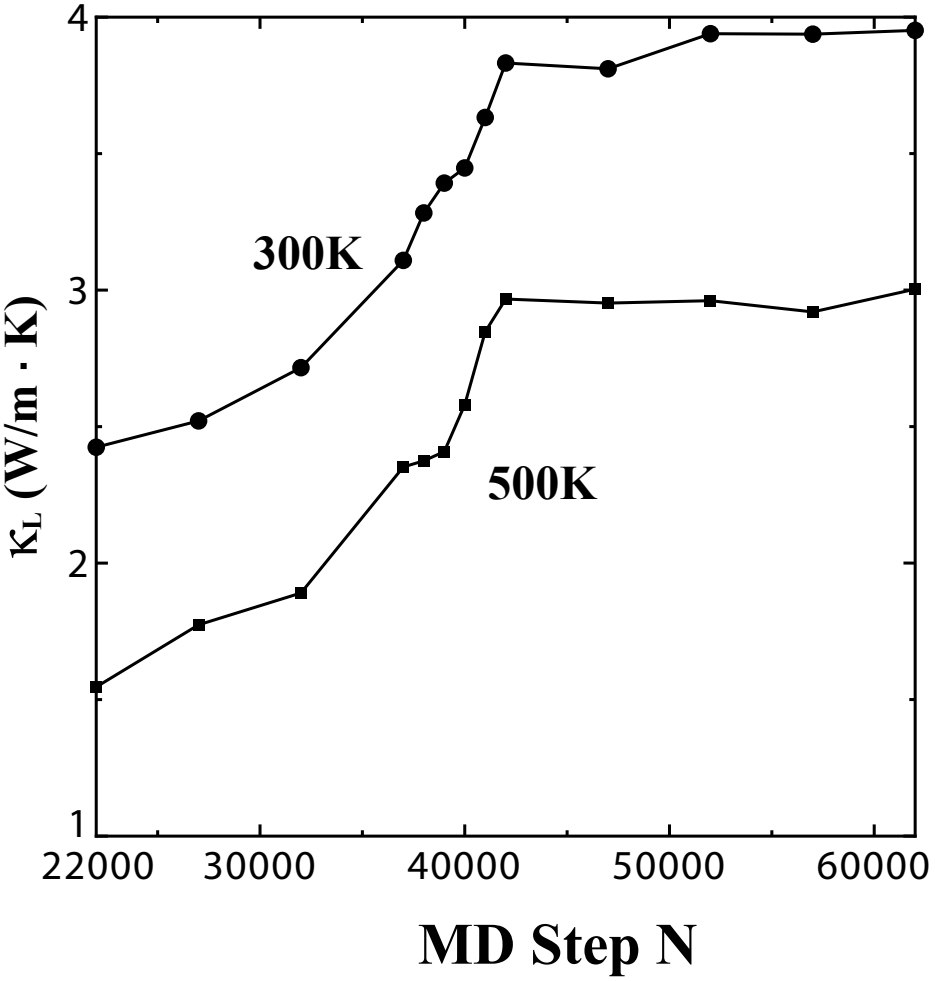

Fig.3 T. Chonan and S. Katayama

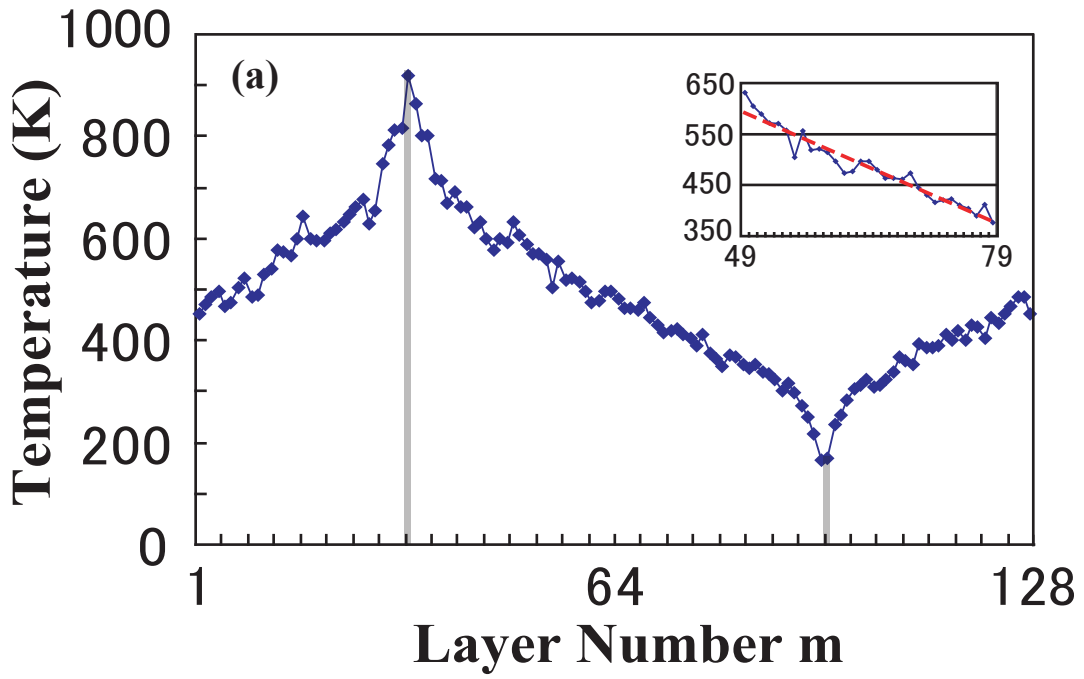

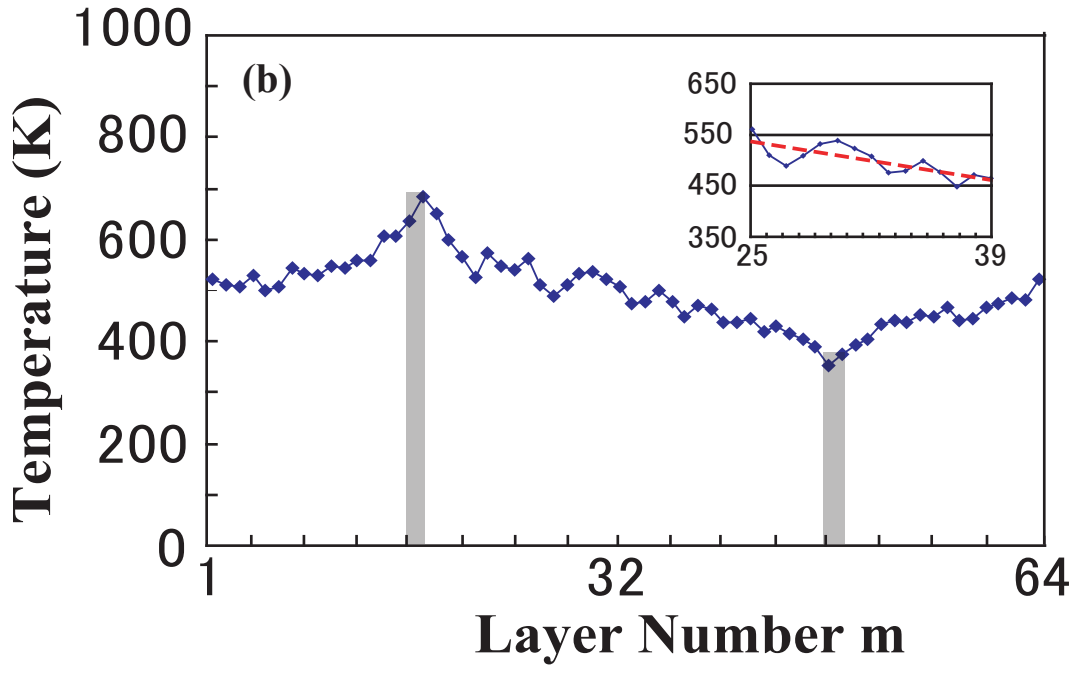

Fig.4 T. Chonan and S. Katayama

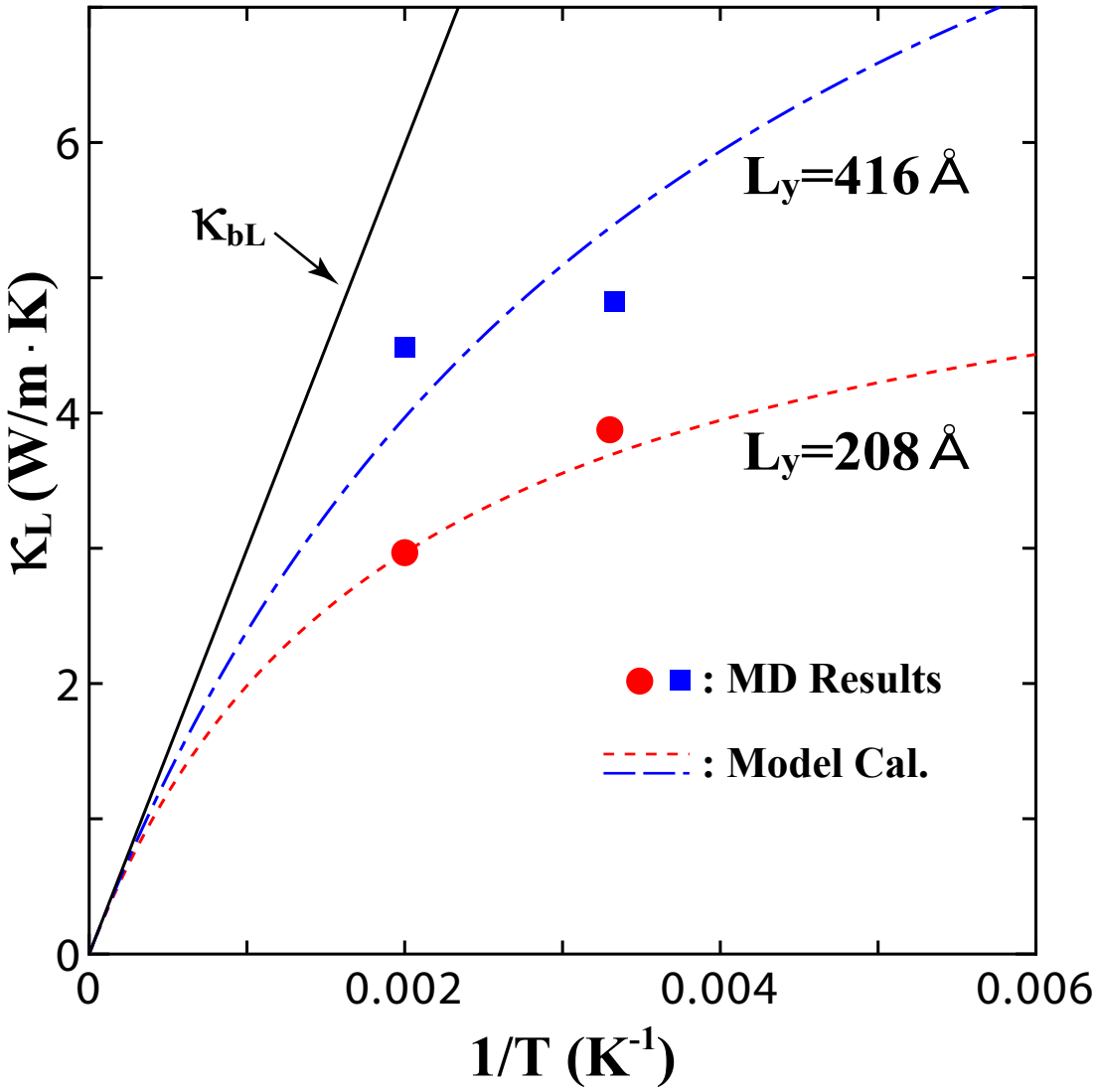

Fig.5 T. Chonan and S. Katayama

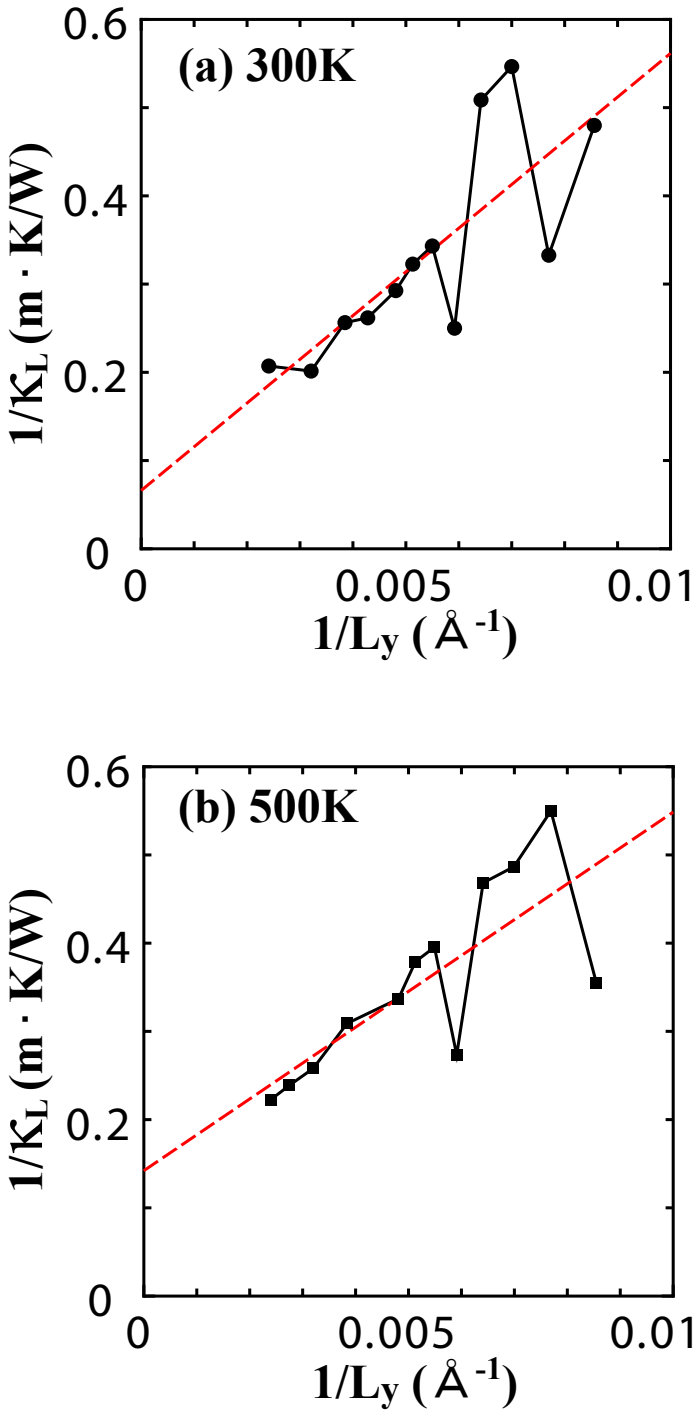

Fig.6 T. Chonan and S. Katayama

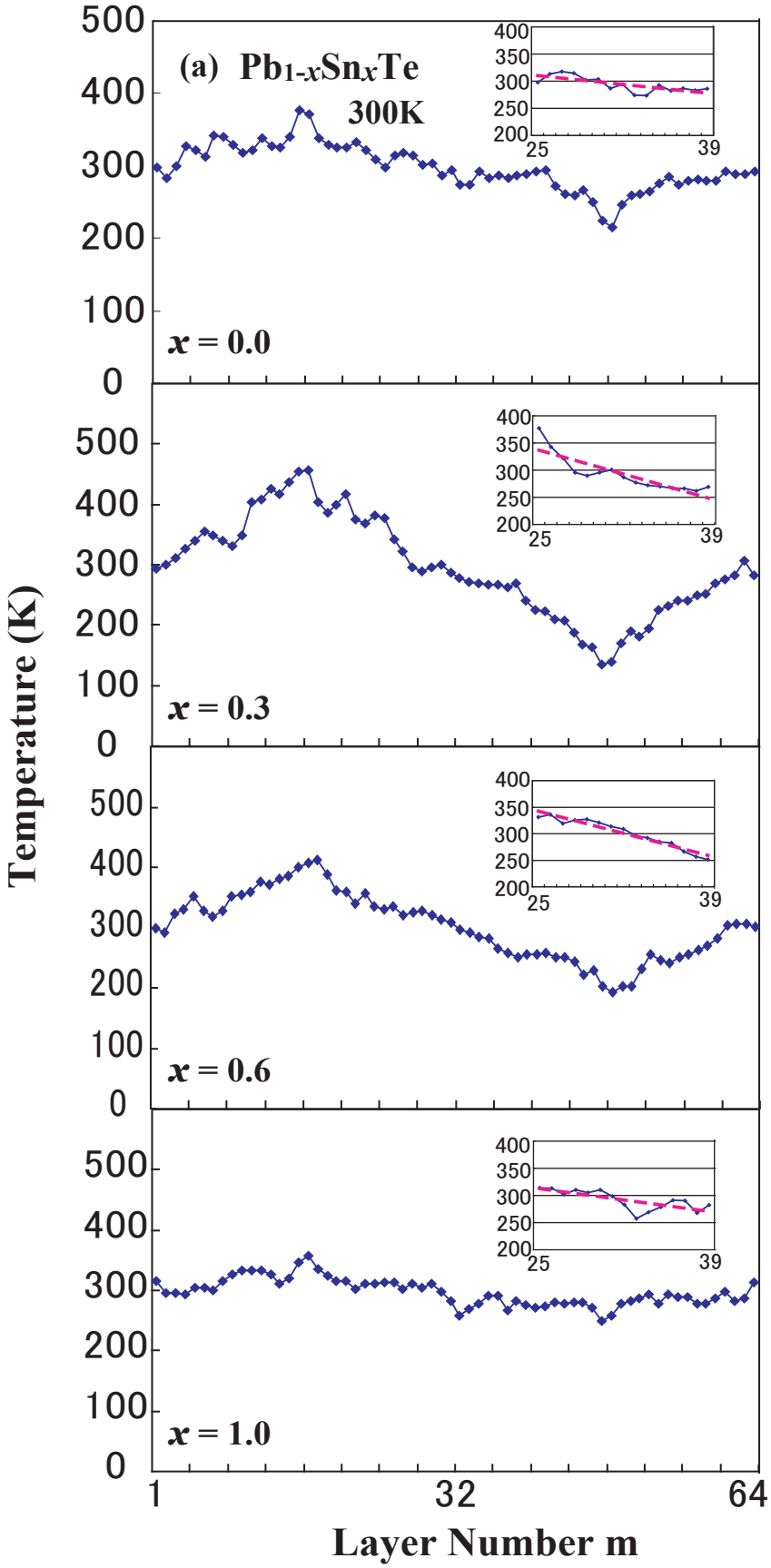

Fig.7 (a) T. Chonan and S. Katayama

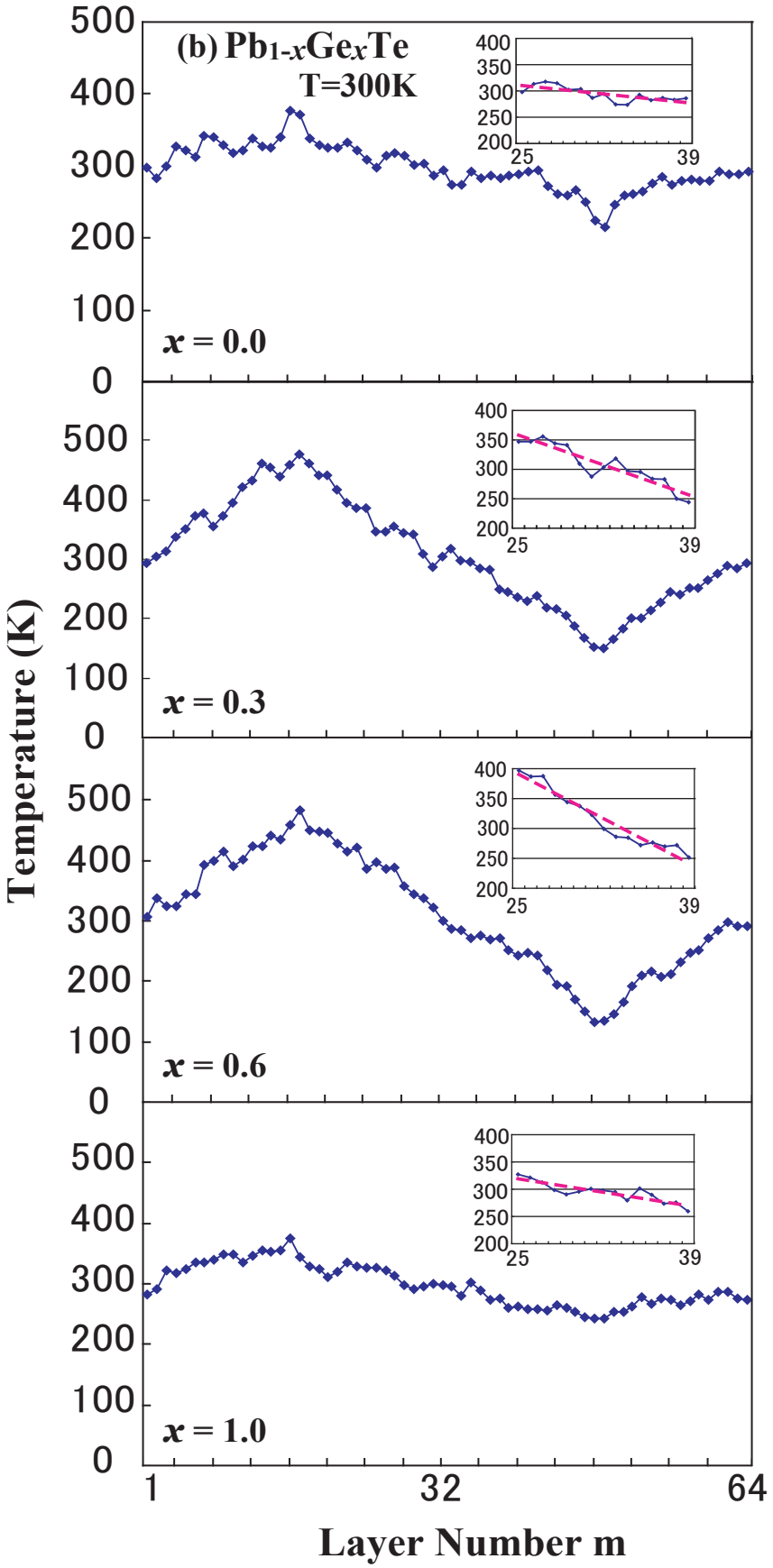

Fig.7 (b) T. Chonan and S. Katayama

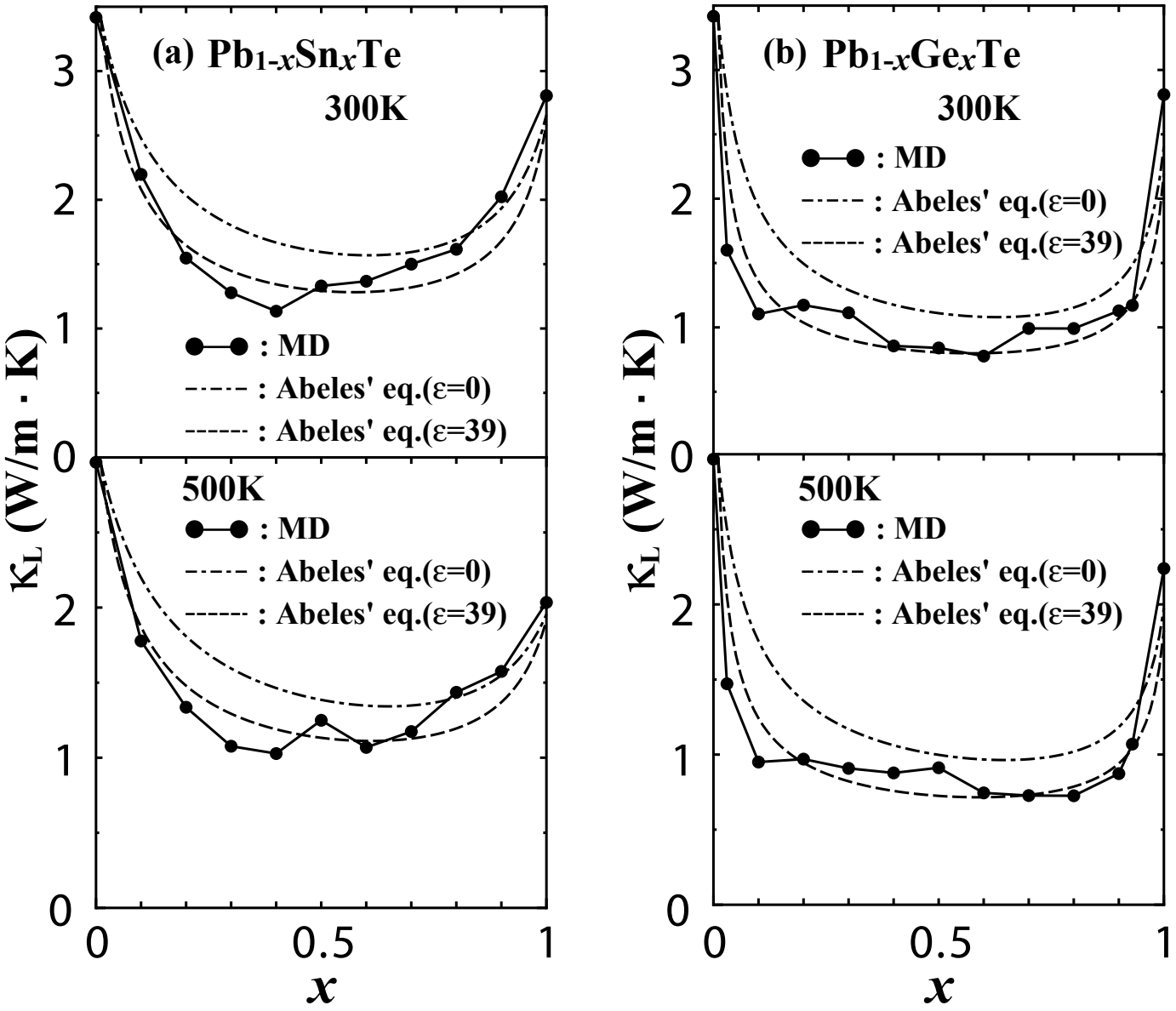

Figs. 8(a), (b) T. Chonan and S. Katayama